J. Fluid Mech. (1966), *vol.* 26, *part* 3, *pp.* 607–637
Printed in Great Britain

The refraction of a plane shock wave at a gas interface

By L. F. HENDERSON
Department of Mechanical Engineering, University of Sydney

(Received 3 January 1966)

The paper deals with the refraction of a plane shock wave by an interface between two different gases. It is shown that the equations of motion can be reduced to a single polynomial equation of degree 12. Detailed numerical results are presented for the air–CH_4 and the air–CO_2 interfaces, which are respectively 'slow–fast' and 'fast–slow' combinations. When the results are compared with experiment good agreement is obtained. The numerical data are multi-valued, but it is found that it is always the weakest solution that agrees with the experimental data. The multiple roots of the equation are often found to be associated with the appearance of degenerate and irregular wave systems and some attempt is made to analyse and discuss these systems.

1. Introduction

Previous papers (Henderson 1964, 1966) have dealt with the interaction of plane shock waves meeting at a point in a perfect gas, and it was found that the equations of motion could be reduced to a single polynomial equation of degree 10. The objective of the present paper is to apply the same methods to the regular refraction of a plane shock wave at a gas interface and in this case it is shown that the polynomial is of degree 12. Following the analysis, detailed numerical results are presented for the air–CH_4 and air–CO_2 interfaces. These gas combinations were selected because the theory could then be compared with some experimental work published by Jahn (1956). The numerical results show that when a physically significant root or solution exists then it is multi-valued; for example, the number of roots m of physical interest for the air–CH_4 interface is either $m = 0$, or 2, but for the air–CO_2 interface it is either $m = 0, 2$, or 4. Still more solutions can be obtained by considering the regular refraction with a reflected expansion wave. The magnitude or strength of a solution may be conveniently measured by the strength of the transmitted shock, and the solutions can then be arranged as an ordered set of ascending order of magnitude. If the set is then compared with experiment it is found that it is always the weakest member of it that actually appears.

The discussion is based upon the methods developed by Guderley (1947, 1962) wherein the flow is mapped simultaneously in the physical (x, y) and hodograph $(\delta, P/P_0)$ planes and then a particular sequence of events is deduced by slowly and continuously changing the boundary conditions. In this way the multiple roots of the polynomial are often found to be associated with the onset of a variety

of degenerate and irregular wave systems and some use is made of this information in an attempt to analyse and discuss the irregular systems photographed by Jahn.

2. Jahn's experiments

The experiments were carried out in a shock tube which had the essential features shown in figure 1. The refraction cell was filled with either methane or carbon dioxide at low pressure, and the space outside the cell was filled with air at the same pressure. The gases were prevented from mixing at the interface by means of an extremely tenuous membrane with an approximate mass per unit area of $5\,\mu g$ per cm^2. There were several reasons for selecting these gas combinations. Thus at the same temperature the speed of sound in air is smaller than the

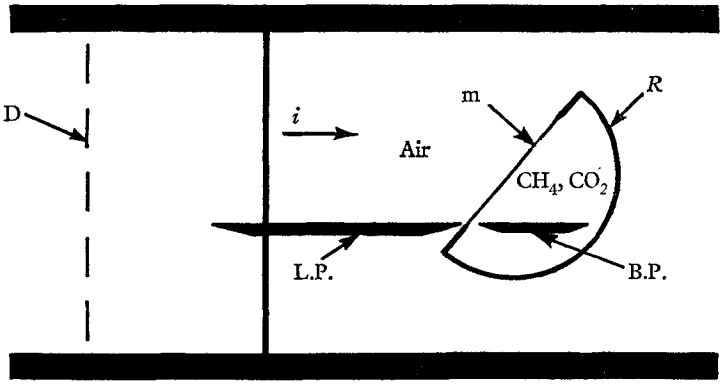

FIGURE 1. Essential features of the shock tube used in Jahn's experiments. *i*, Incident shock; m, membrane; *R*, refraction cell; B.P., back plate; D, diaphragm; L.P., leading plate.

speed of sound in methane and therefore it was expected that the air–CH_4 combination would be typical of the refraction of a plane shock propagating from a 'slower' to a 'faster' medium. By contrast the air–CO_2 interface should be typical of a 'fast–slow' refraction. More extreme gas combinations such as air–helium and air–freon would be expected to display the phenomena more clearly but they could not be used conveniently because of practical difficulties with the membrane. A further reason for selecting air–CH_4 and air–CO_2 for study was that the results could be compared with some theoretical work that had been done on these combinations by Polachek & Seeger (1951).

The incident shock *i* was formed in the usual way by rupturing a diaphragm and it then propagated down the tube to strike the membrane at a given angle of incidence α. The wave pattern was photographed with the help of an interferometer and from this information the wave angles and density distribution could be measured. The phenomena were explored using two shock strengths, namely $\xi = (P_0/P_1) = 0{\cdot}3$ (strong) and $\xi = 0{\cdot}85$ (weak) and for angles of incidence in the range $\alpha = 0°$ or normal incidence to $\alpha = 90°$ or glancing incidence. The observed wave patterns can be conveniently classified into two groups. First, there is the

regular group, figure 2, which is characterized by a well-defined refraction point and by the property that all the waves lie on straight rays that radiate from this point. In this group the reflected wave may be either a shock r or a Prandtl–Meyer expansion e, but the transmitted wave is always a shock t. The second

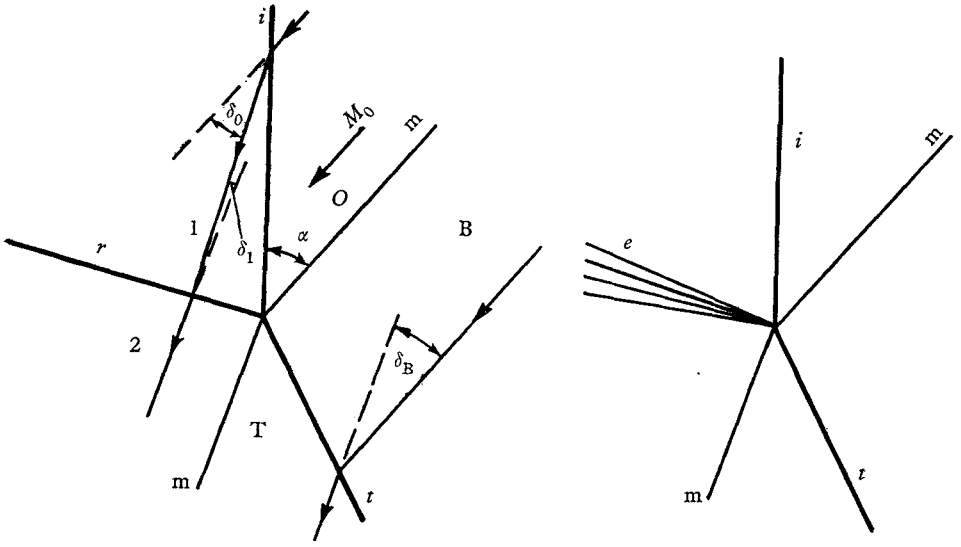

FIGURE 2. The wave systems in the regular refraction group.

group are collectively called the irregular refractions and are merely the wave systems that are not covered by the above definition; some of the examples observed by Jahn are sketched in figures 12(f), 13(c), (e), (f), (g), and 15(f). The data obtained from the experiments on the regular refractions are reproduced in figures 3, 4 and 5. Here the size of the symbols indicates the range of the experimental error. When Jahn compared his results with those of Polachek & Seeger, he found it necessary to make a number of corrections. For example, Polachek & Seeger had used somewhat unrealistic values for the gas properties† and Jahn made some approximations to correct for this effect. He also made a number of corrections to the experimental data; in particular he corrected for the fact that a certain amount of mixing of the gases at the interface could not be prevented. After these adjustments there was satisfactory agreement between theory and experiment. A small amount of data has also been published on the irregular refraction at the air–CH_4 interface and this has been reproduced in figure 6.

3. Analysis of the regular refraction with a reflected shock

It will be assumed that the wave pattern is stationary and that every point on it propagates at the same absolute velocity. In particular the velocity of the incident and transmitted shocks along the interface will be equal and therefore

$$v_{\text{air}} = v_{CH_4,CO_2}.$$

† The ratio of specific heats was taken to be $\gamma = \frac{4}{3}$ for both CH_4 and CO_2.

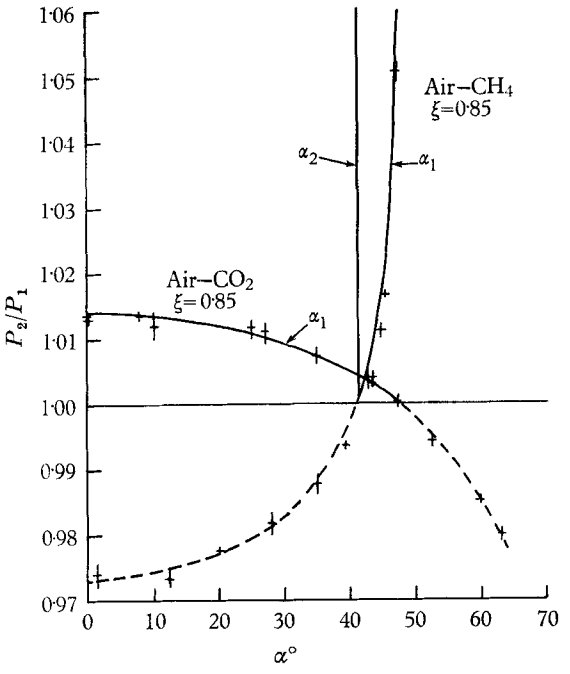

FIGURE 3. Theoretical and experimental results for regular shock-wave refraction with $\xi = 0{\cdot}85$. ——, present theory; – – –, adjusted Polachek & Seeger theory; +, Jahn's experimental data.

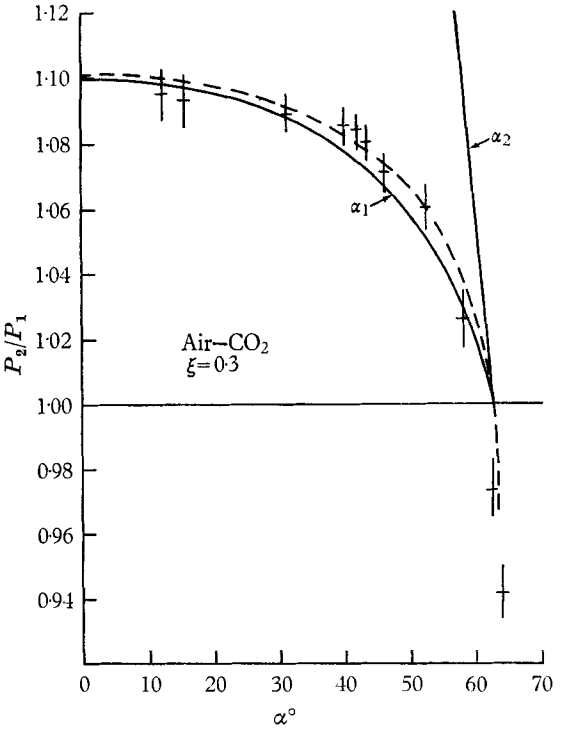

FIGURE 4. Theoretical and experimental results for regular shock-wave refraction with $\xi = 0{\cdot}3$. ——, present theory; – – –, adjusted Polachek & Seeger theory; +, Jahn's experimental data.

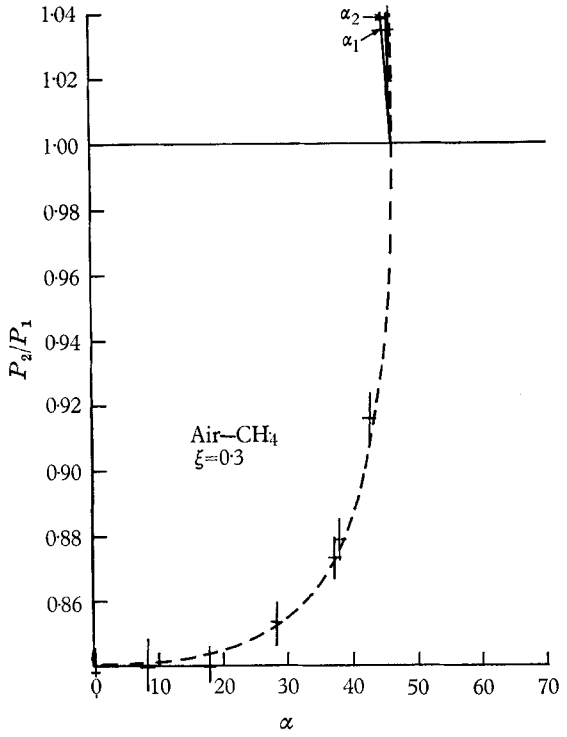

FIGURE 5. Theoretical and experimental results for regular shock-wave refraction with $\xi = 0{\cdot}3$. ——, present theory; – – –, adjusted Polachek & Seeger theory; +, Jahn's experimental data.

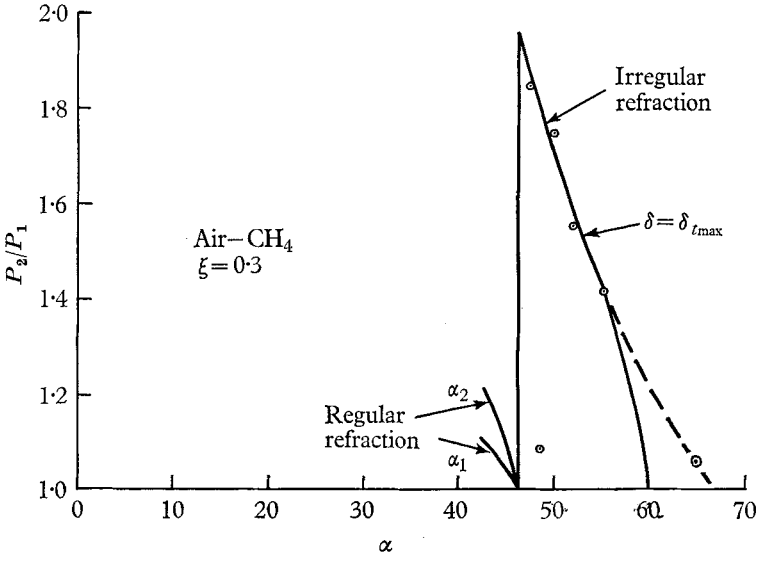

FIGURE 6. Theoretical and experimental results for irregular shock-wave refraction with $\xi = 0{\cdot}3$. ——, three-shock theory; ⊙, Jahn's experimental data; – – –, curve of best fit through Jahn's data.

The speed of sound will depend on the nature of the gas and its temperature $a = [\gamma RT/\mathscr{M}]^{\frac{1}{2}}$, but it will be supposed that the temperatures of the undisturbed gases will be everywhere the same. The following relations may now be obtained between the upstream Mach numbers of the incident and transmitted shocks:

$$M_{\mathrm{CH_4,CO_2}} = M_{\mathrm{air}}\left[\frac{\gamma_{\mathrm{air}}}{\gamma_{\mathrm{CH_4,CO_2}}}\frac{\mathscr{M}_{\mathrm{CH_4,CO_2}}}{\mathscr{M}_{\mathrm{air}}}\right]^{\frac{1}{2}}. \tag{1a}$$

The gas constants were selected after consulting McBride *et al.* (1963), and Hilsenrath *et al.* (1960) and were as shown in table 1. Equation (1*a*) then becomes

$$M_{\mathrm{CH_4,CO_2}} = 0{\cdot}7711,\ 1{\cdot}284_5 M_{\mathrm{air}}. \tag{1b}$$

The flow that exists in a shock tube is referred to as pseudo-stationary or self-similar, and has the property that the wave pattern grows uniformly with time. Sternberg (1959) has compared the equations for stationary and pseudo-stationary flow and found that in small local regions the pseudo-stationary

	Air	CH_4	CO_2
Ratio specific heats (γ)	1·402	1·303	1·288
Mol. wt. ($\mathscr{M}$)	29·02	16·04	44·01

TABLE 1.

equations reduce to the stationary equations. It will be assumed here that the analysis will be valid for both types of flow in the neighbourhood of the refraction point. It will also be assumed that the gases are perfect, inviscid, and of constant specific heats. The following equations are now available from one-dimensional shock theory:

$$\tan\delta_{0,1,B} = \frac{(P_{1,2,T}/P_{0,1,B})-1}{1+\gamma_{0,0,B}M^2_{0,1,B}-(P_{1,2,T}/P_{0,1,B})} \times\left[\frac{\{2\gamma_{0,0,B}/(\gamma_{0,0,B}+1)\}M^2_{0,1,B}-(\gamma_{0,0,B}-1)/(\gamma_{0,0,B}+1)-(P_{1,2,T}/P_{0,1,B})}{(\gamma_{0,0,B}-1)/(\gamma_{0,0,B}+1)+(P_{1,2,T})/(P_{0,1,B})}\right]^{\frac{1}{2}}, \tag{2}$$

and

$$\frac{1+\frac{1}{2}(\gamma_0-1)M_0^2}{1+\frac{1}{2}(\gamma_0-1)M_1^2} = \frac{(\gamma_0+1)/(\gamma_0-1)+(P_1/P_0)}{(\gamma_0+1)/(\gamma_0-1)+(P_0/P_1)}. \tag{3}$$

In addition there are the following continuity conditions to be satisfied at the interface

$$\delta_B = \delta_0+\delta_1, \tag{4}$$

$$P_T/P_B = (P_1/P_0)\,(P_2/P_1). \tag{5}$$

Equations (1) to (5) will be collectively described as the equations of motion; there are seven of them altogether and they involve twelve variables

$$(\gamma_{0,B},\quad \mathscr{M}_{\mathrm{CH_4,CO_2}}/\mathscr{M}_{\mathrm{air}},\quad M_{0,1,B},\quad P_{1,2,T}/P_{0,1,B},\quad \delta_{0,1,B}).$$

Thus to define a solution or set of solutions it is necessary to assign values to five of the variables and for this purpose it will be convenient to select $\gamma_{0,B}$,

$\mathscr{M}_{CH_4,CO_2}/\mathscr{M}_{air}$, P_1/P_0, M_0. A particular set of values of these variables will be the initial conditions corresponding to a set of solutions.

The equations of motion can now be reduced to a single polynomial equation of degree 12, where the polynomial variable is P_T/P_B. The method has been given before (Henderson 1964) and by this means explicit expressions may be obtained for computing the coefficients exactly.† There are now 12 roots or solutions to be considered but a root must satisfy at least two criteria before it can be regarded as having physical significance. These are:

(i) The root must be real because no meaning can be attached to an unreal value of P_T/P_B.

(ii) $P_T/P_B \geqslant P_1/P_0 \geqslant 1$; this condition is necessary to avoid thermodynamically impossible expansion shocks.

Occasionally it is found that for particular initial conditions one wave in the system will degenerate to a Mach line. Such a result will be thought of as physically trivial. The integers m_{CH_4} and m_{CO_2} will be used to indicate the number of physically significant and non-trivial roots.

A complete picture of the physical meaning of the polynomial requires a knowledge of all the physically significant single and multiple roots. The necessary data were obtained from a computer using the exact expressions. The part of the data that satisfies the above tests has been plotted in figures 7 and 8. It will be noted that an ordinate line $P_1/P_0 = \text{const.}$ will cut the curves for the air–CH_4 refraction in either $m_{CH_4} = 0$, or 2 places, while for the air–CO_2 refraction it will cut in either $m_{CO_2} = 0$, 2, or 4 places, a fact that displays the multiple nature of the solutions for given initial conditions. A double root occurs where an ordinate line is tangent to a curve. These roots have been separately computed and the results are presented in figures 9 and 10.

The equations of motion can also be solved graphically in the hodograph $(\delta, P/P_0)$ plane using the well-known shock polar method, figures 11–17. The real roots of the polynomial are then represented by the ordinates of the polar intersections. The polar diagram shows that the polynomial always has a double root‡ at $P_T/P_B = 1$. This may be seen at once by noting that the polars for the incident I and reflected III shocks pass through each other's double point D_1 and D_2 (Henderson 1964). Now one of these points D_1 is at (0, 1) and because the double point of the CH_4 or CO_2 polar II also passes through D_1 then the double root $(P_T/P_B - 1)^2$ must exist. Although it is not physically significant it saves a substantial amount of work on the computer if this double root is removed by synthetic division. The polar diagrams have several useful functions—for example, they facilitate the understanding of the polynomial root structure and also help in the physical interpretation of these roots, but perhaps their most useful function is that they can be used to construct an orderly sequence of events for gradually changing boundary conditions. Of particular interest will be the sequence that can be deduced by imagining that the polar for the reflected

† The original version of the present paper contained the expressions as an appendix but lack of space in publication forced them to be deleted. They are available on request from the author. L.F.H.

‡ I am indebted to Mr McPherson for pointing the double root out to me.

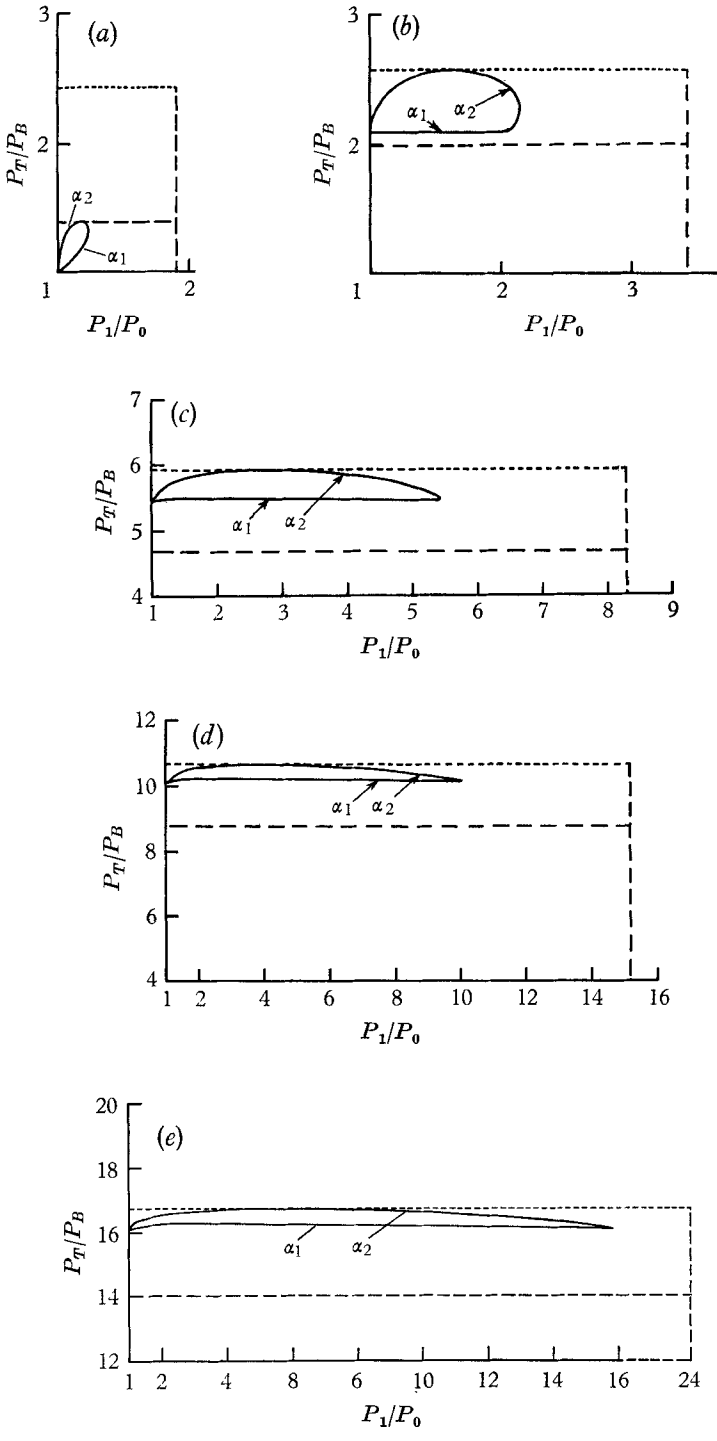

FIGURE 7. Physically significant roots of the polynomial equation for the regular refraction of a plane shock at the air–CH_4 interface. ——, polynomial root line; – –, sonic line; ----, normal shock line. (*a*) $M_0 = 1{\cdot}5$; (*b*) $M_0 = 2{\cdot}0$; (*c*) $M_0 = 3{\cdot}0$; (*d*) $M_0 = 4{\cdot}0$; (*e*) $M_0 = 5{\cdot}0$.

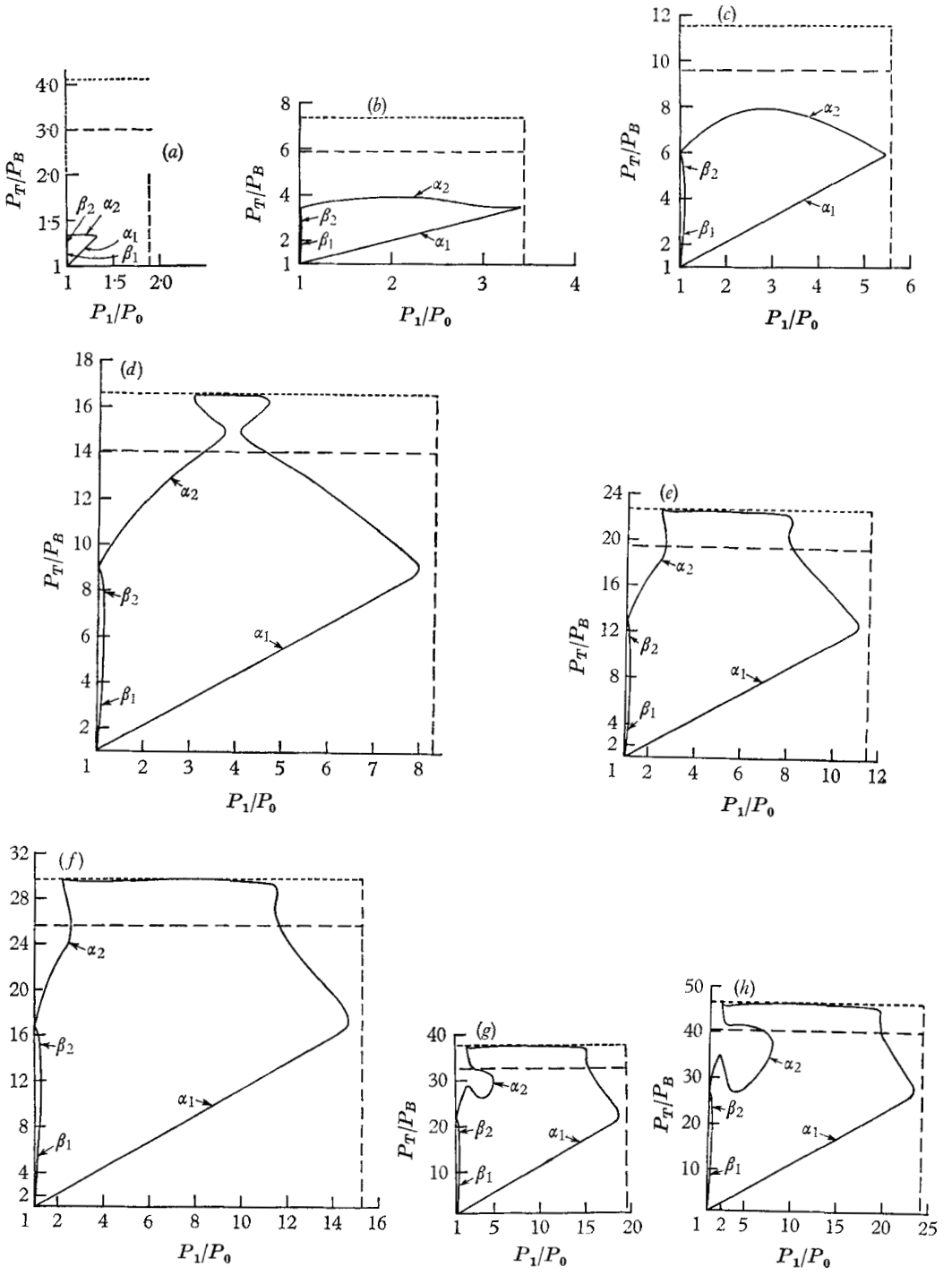

FIGURE 8. Physically significant roots of the polynomial equation for the regular refraction of a plane shock at the air–CO_2 interface. ——, polynomial root line; – –, sonic line; ----, normal shock line. (*a*) $M_0 = 1{\cdot}5$; (*b*) $M_0 = 2{\cdot}0$; (*c*) $M_0 = 2{\cdot}5$; (*d*) $M_0 = 3{\cdot}0$; (*e*) $M_0 = 3{\cdot}5$; (*f*) $M_0 = 4{\cdot}0$; (*g*) $M_0 = 4{\cdot}5$; (*h*) $M_0 = 5{\cdot}0$.

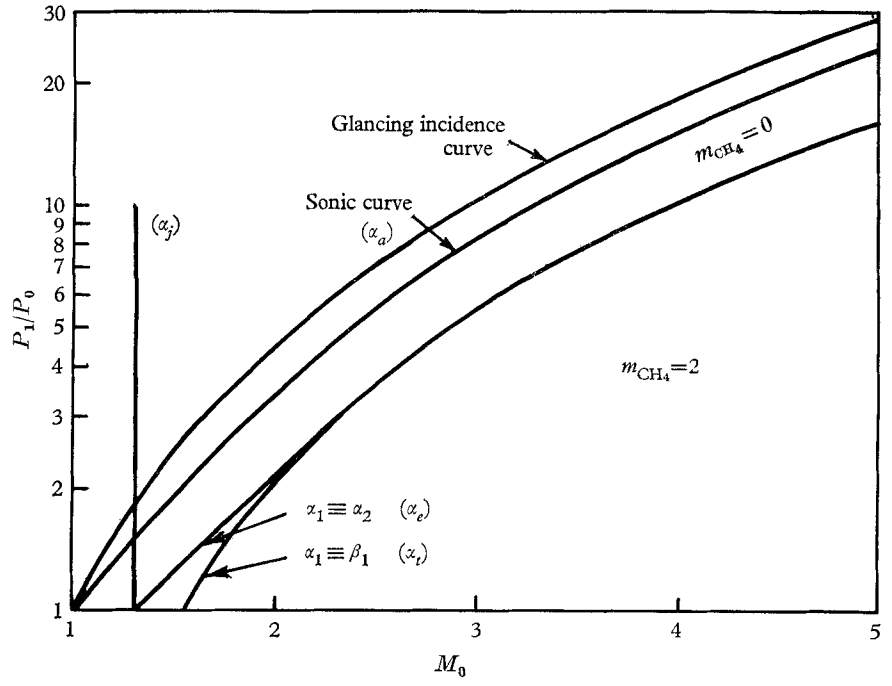

FIGURE 9. Multiple root lines and other critical curves for the air–CH_4 interface.

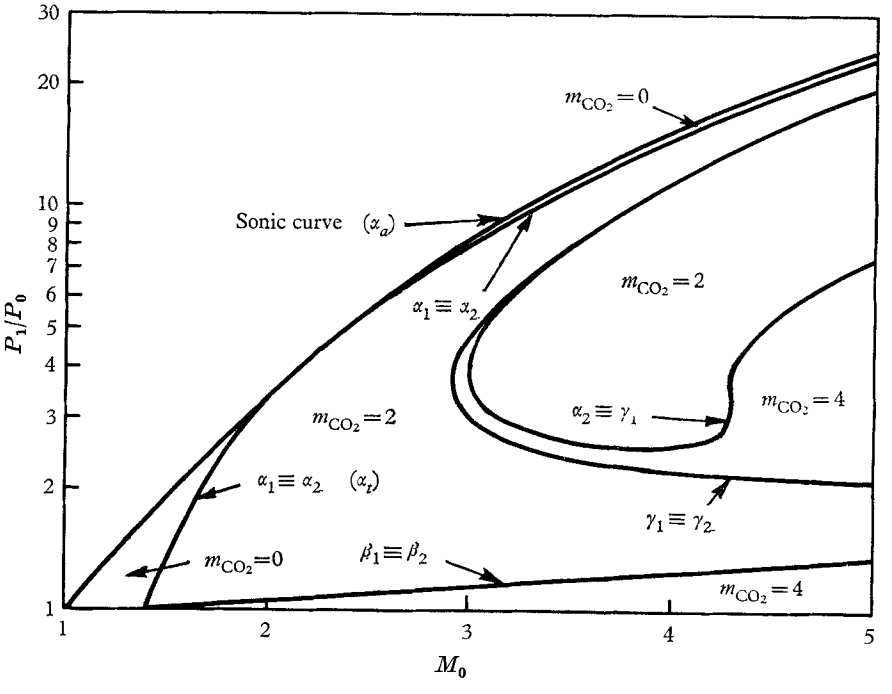

FIGURE 10. Multiple root lines and other critical curves for the air–CO_2 interface.

shock III is initially in coincidence with the polar for the incident shock I and is then gradually and continuously displaced from it. Physically this is equivalent to the incident shock being initially a Mach line and then gradually strengthening into a shock of increasing intensity. During this process the Mach number M_0 upstream of the incident shock is held constant.

4. Regular refraction at the air–methane interface

From equation (1*b*) it may be concluded that the methane polar II does not exist† over the Mach-number range $M_0 \leqslant 1{\cdot}30$. There are no physically significant roots of the polynomial equation in these circumstances and the appearance of an irregular wave system is therefore to be expected. The limiting condition is represented in figure 9 by the ordinate line $M_0 = 1{\cdot}30$. For the Mach-number range $1{\cdot}30 \leqslant M_0 \leqslant 1{\cdot}55$, it can be shown that the methane polar II is entirely contained inside the air polar I, as in figure 11. This fact may be demonstrated by computing the intersection points between I and II and it is then found that the polars do not intersect until $M_0 \geqslant 1{\cdot}55$, except of course at D_1. If III is now slightly displaced from I as shown in figure 11 (*a*), then in general two polar intersections α_1 and α_2 will be obtained. Physically, both points represent a regular refraction with a reflected shock. The hodograph diagram shows that the pressure ratio across the transmitted shock is smaller for the α_1 solution than for the α_2 solution and for this reason the α_1 solution will be defined to be the weaker of the two solutions. It will be convenient to arrange the solutions as an ordered set of numbers in ascending order of magnitude thus (α_1, α_2). With continuous displacement of III, α_1 and α_2 approach each other, figure 11 (*b*), and eventually coincide to form a double point as in figure 11 (*c*). This coincidence will be denoted by $\alpha_1 \equiv \alpha_2$ and it evidently corresponds to a double root of the polynomial. If displacement continues any further α_1 and α_2 will become unreal and there will then be no solutions of physical interest. This again suggests the appearance of an irregular wave system but a discussion of it will be deferred for the present. It therefore appears that the physical significance of the double root $\alpha_1 \equiv \alpha_2$ is that it is a boundary between regular and irregular wave systems. The root was determined on the computer and the results are shown in figure 9.

Over the Mach-number range $1{\cdot}55 \leqslant M_0 \leqslant 2{\cdot}25$ the methane polar II lies partly outside the air polar I and this leads to the type of sequence shown in figure 12. When III is displaced from I by a small amount, then once more there are two intersections of physical interest (α_1, α_2). If polar III is extended below D_2 then an extra solution β_1 is obtained; although this solution is not physically significant it is important in the way it forms a double point with α_1, as will be shown presently. It is also possible to construct a graphical solution in which the wave system contains a reflected Prandtl–Meyer expansion instead of a reflected shock. This may be done with the help of the characteristic c_1 which passes through the point D_2. This curve intersects II at the point ϵ_1 and the ordered set now becomes $(\epsilon_1, \alpha_1, \alpha_2)$, figure 12 (*a*). The polynomial equation is not of course valid for a solution of the ϵ_1 type and any discussion of it given here must be

† Because, from equation (1*b*), $M_{CH_4} \leqslant 1$ when $M_{air} \leqslant 1{\cdot}30$.

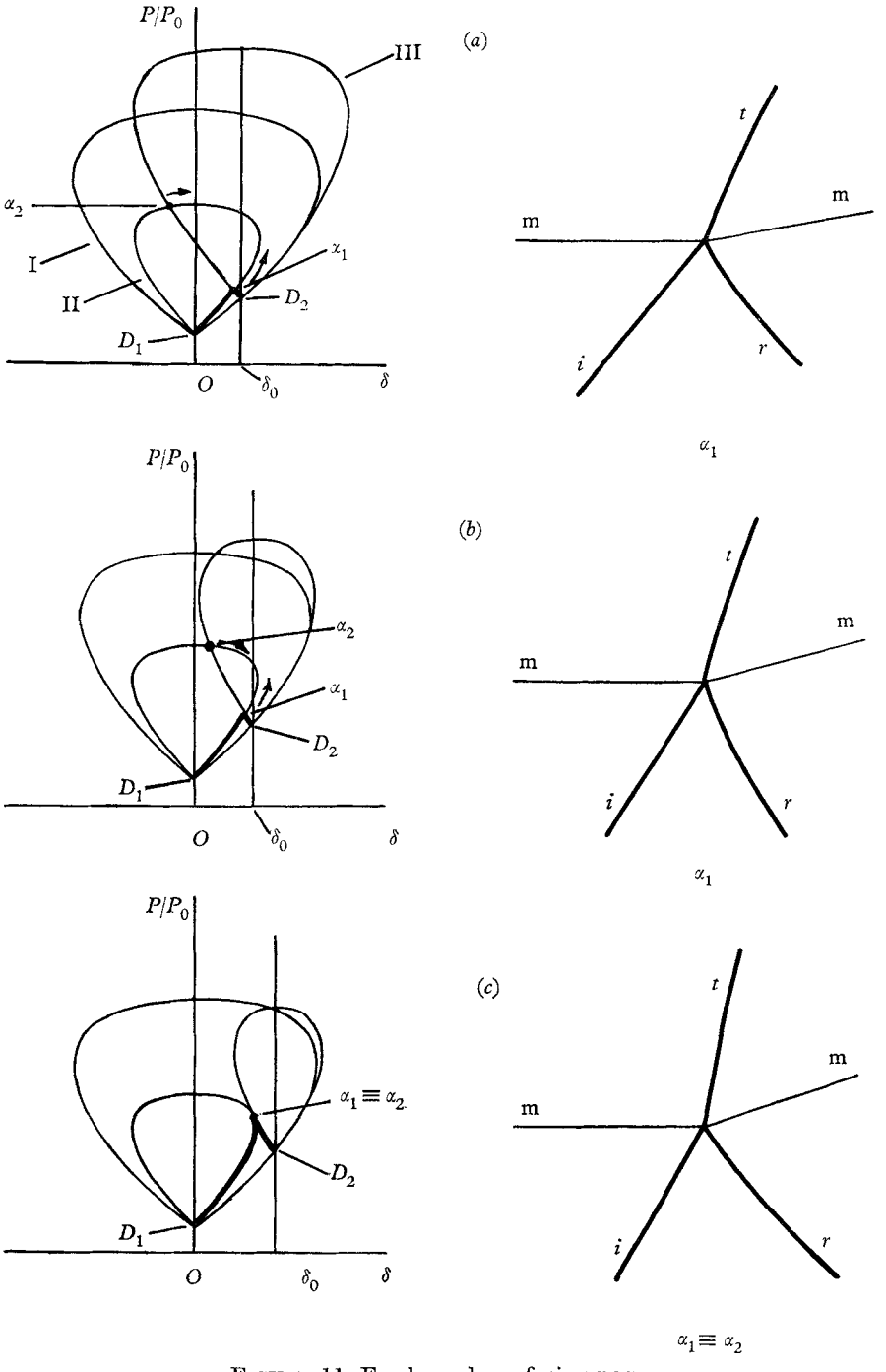

FIGURE 11. For legend see facing page.

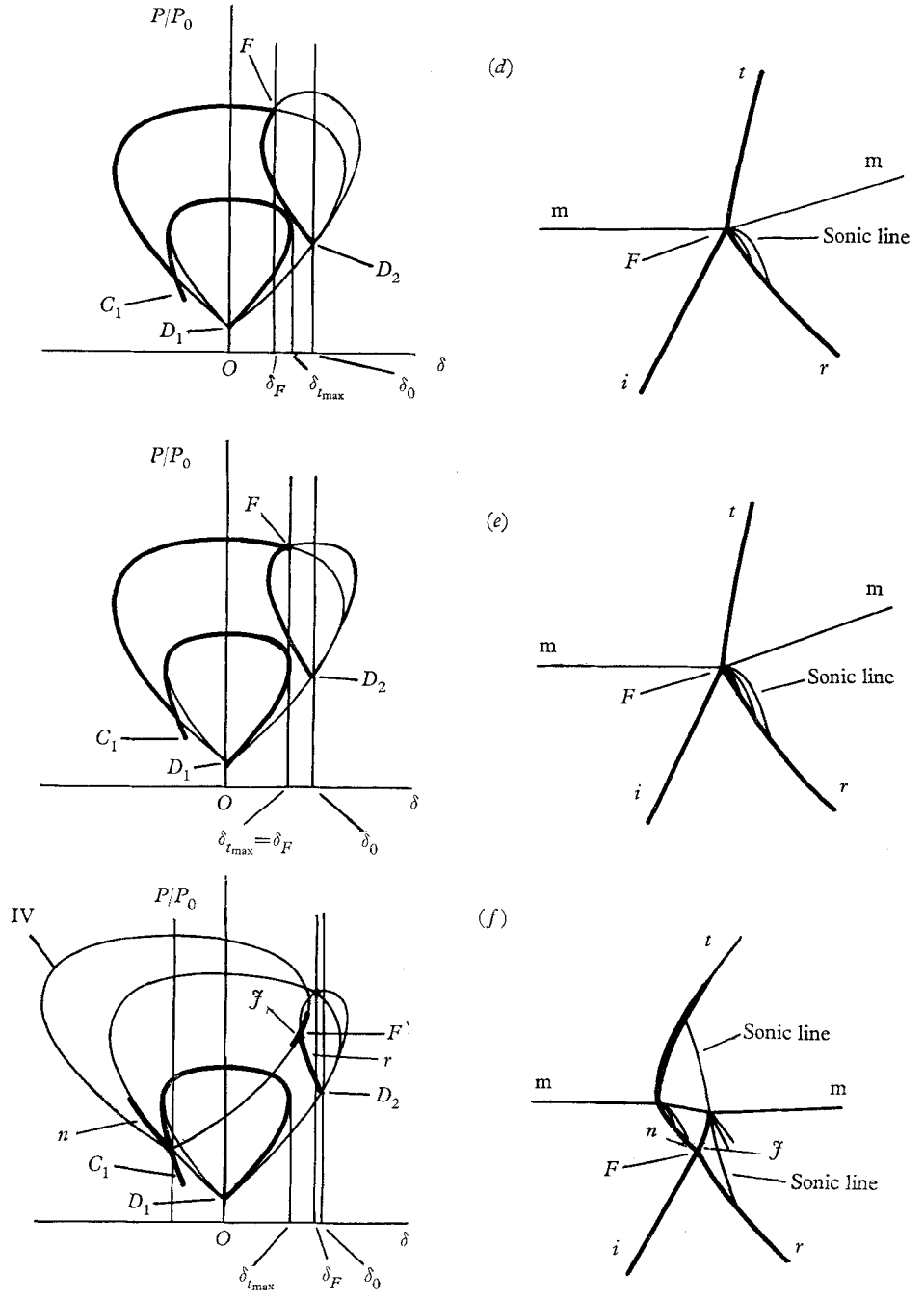

FIGURE 11. Sequence of events resulting from the displacement of polar III from polar I for the refraction of a plane shock i at an air–methane interface in the Mach-number range $1{\cdot}30 \leqslant M_0 \leqslant 1{\cdot}55$.

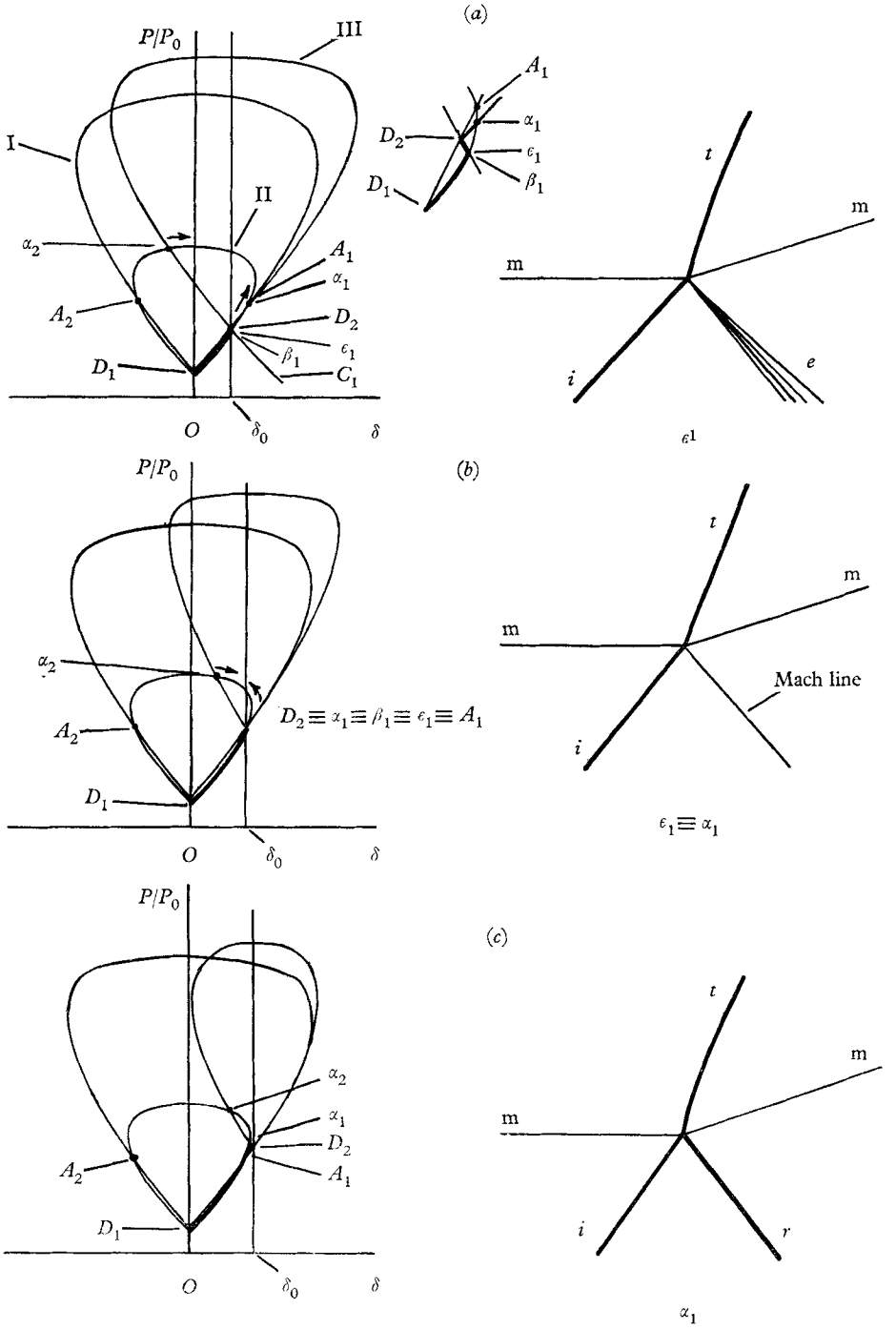

FIGURE 12. For legend see facing page.

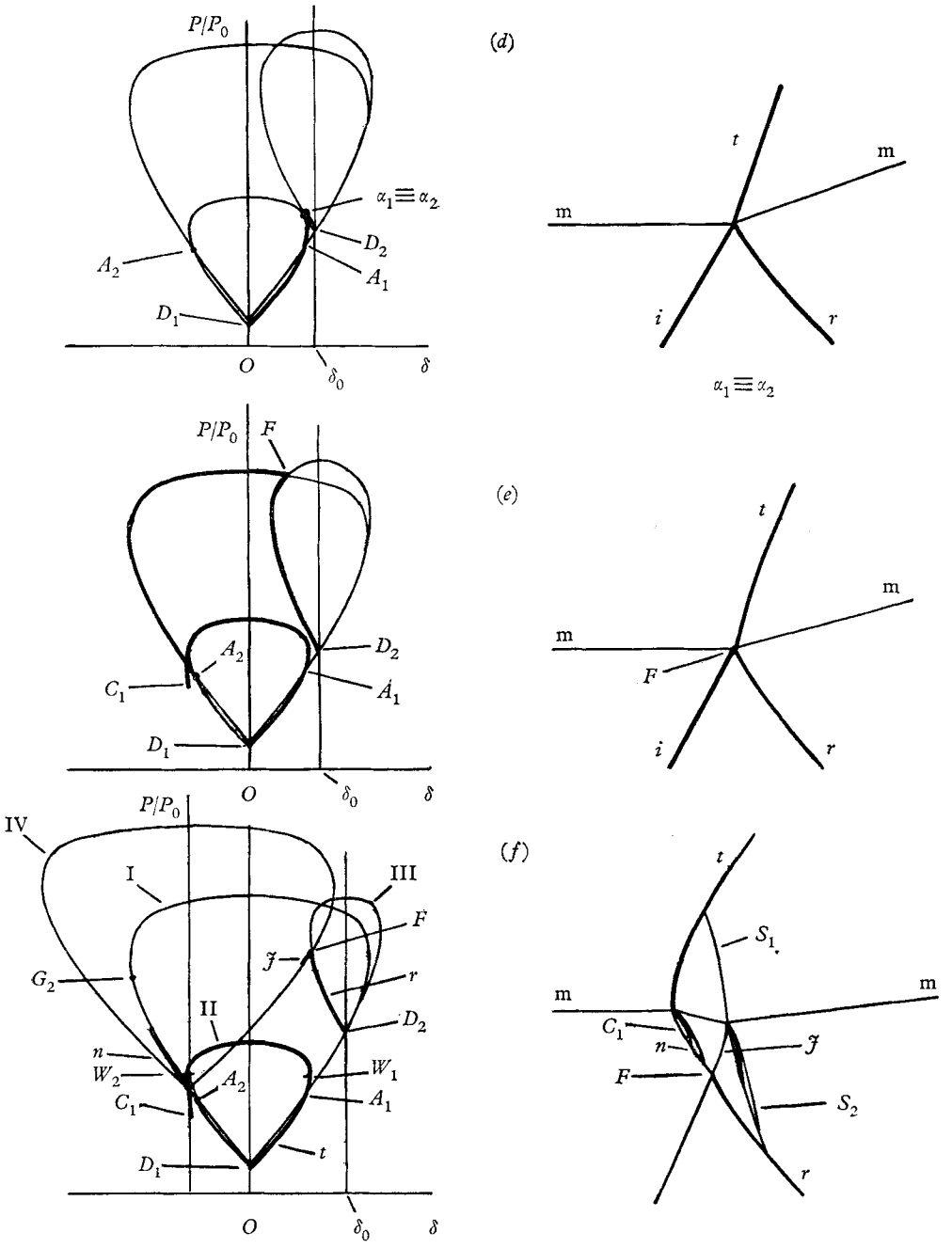

FIGURE 12. Sequence of events resulting from the displacement of polar III from polar I for the refraction of a plane shock i at an air–methane interface in the Mach-number range $1{\cdot}55 \leqslant M_0 \leqslant 2{\cdot}25$.

mainly qualitative. The points β_1 and ϵ_1 are usually so close together that they cannot be separately distinguished. As displacement continues, the point D_2 eventually reaches A_1 which is one of the intersection points between I and II. When this happens the point D_2 is simultaneously joined by the solutions α_2, β_1 and ϵ_1 so that there is the coincidence $D_2 \equiv \alpha_1 \equiv \beta_1 \equiv \epsilon_1 \equiv A_1$, as shown in figure 12(*b*). For α_1, β_1 and ϵ_1 the physical consequence is that the reflected wave has now degenerated to a Mach line. With further displacement, both the β_1 and ϵ_1 solutions become unreal but the α_1 solution strengthens so that the set is now (α_1, α_2). It may now be concluded that the physical significance of the coincidence $D_2 \equiv \alpha_1 \equiv \beta_1 \equiv \epsilon_1 \equiv A_1$ is that it represents the boundary between a regular refraction with a reflected expansion and a regular refraction with a reflected shock. The double root line $\alpha_1 \equiv \beta_1$ has been determined on the computer and the results are shown in figure 9. With further displacement α_1 and α_2 approach and then coincide $\alpha_1 \equiv \alpha_2$. The resulting double-root line is merely part of the one found in the range $1{\cdot}30 \leqslant M_0 \leqslant 1{\cdot}55$ as also shown in figure 9. Finally, with any more displacement α_1 and α_2 become unreal, which again suggests the appearance of an irregular wave system.

From figure 9 it will be noted that the two root lines $\alpha_1 \equiv \alpha_2$ and $\alpha_1 \equiv \beta_1$ coincide when $M_0 \geqslant 2{\cdot}25$. A typical sequence for this condition is shown in figure 13. The ordered set is again $(\epsilon_1, \alpha_1, \alpha_2)$ but the ϵ_1 solution is now co-extensive with the α_1 and α_2 solutions, so that it exists whenever they do. With continuous displacement of D_2 the physical result is that all solutions eventually and simultaneously form a Mach line degeneracy at $D_2 \equiv \alpha_1 \equiv \alpha_2 \equiv \beta_1 \equiv \epsilon_1 \equiv A_1$ and beyond this condition irregular systems are to be expected. There are two other curves in figure 9 of interest. One of them is for the condition where the flow downstream of the incident shock is sonic. Clearly there can be no reflected wave if the flow downstream of the incident shock becomes subsonic and the sonic curve is therefore the limiting condition. The remaining curve is the condition for glancing incidence of the shock i on the interface and along this curve $\alpha = 90°$.

5. Regular refraction at the air–carbon dioxide interface

The first sequence is shown in figure 14 and its characteristic feature is that the air polar I is contained inside the carbon dioxide polar II. This occurs for the Mach-number range $M_0 \leqslant 1{\cdot}38$. The only regular refraction that is now conceivable is ϵ_1 so that in this case there is a unique solution. As the point D_2 is continuously displaced it ultimately reaches the sonic point V on I $D_2 \equiv V$. This means that the flow downstream of the incident shock must now move at sonic speed and furthermore the reflected expansion must degenerate to a sonic Mach line. The sonic curve is plotted in figure 10. No physical meaning can be attached to the regular solution if there is any further displacement of D_2 and once more the appearance of an irregular refraction is implied. The next sequence, figure 15, is typical of the Mach-number range $1{\cdot}38 \leqslant M_0 \leqslant 2{\cdot}0$ and the air polar I is now partly outside the CO_2 polar II. A small displacement of III now yields four intersections so that the ordered set becomes $(\alpha_1, \beta_1, \beta_2, \alpha_2)$. As displacement continues, the coincidence $\beta_1 \equiv \beta_2$ is formed and the corresponding double-root

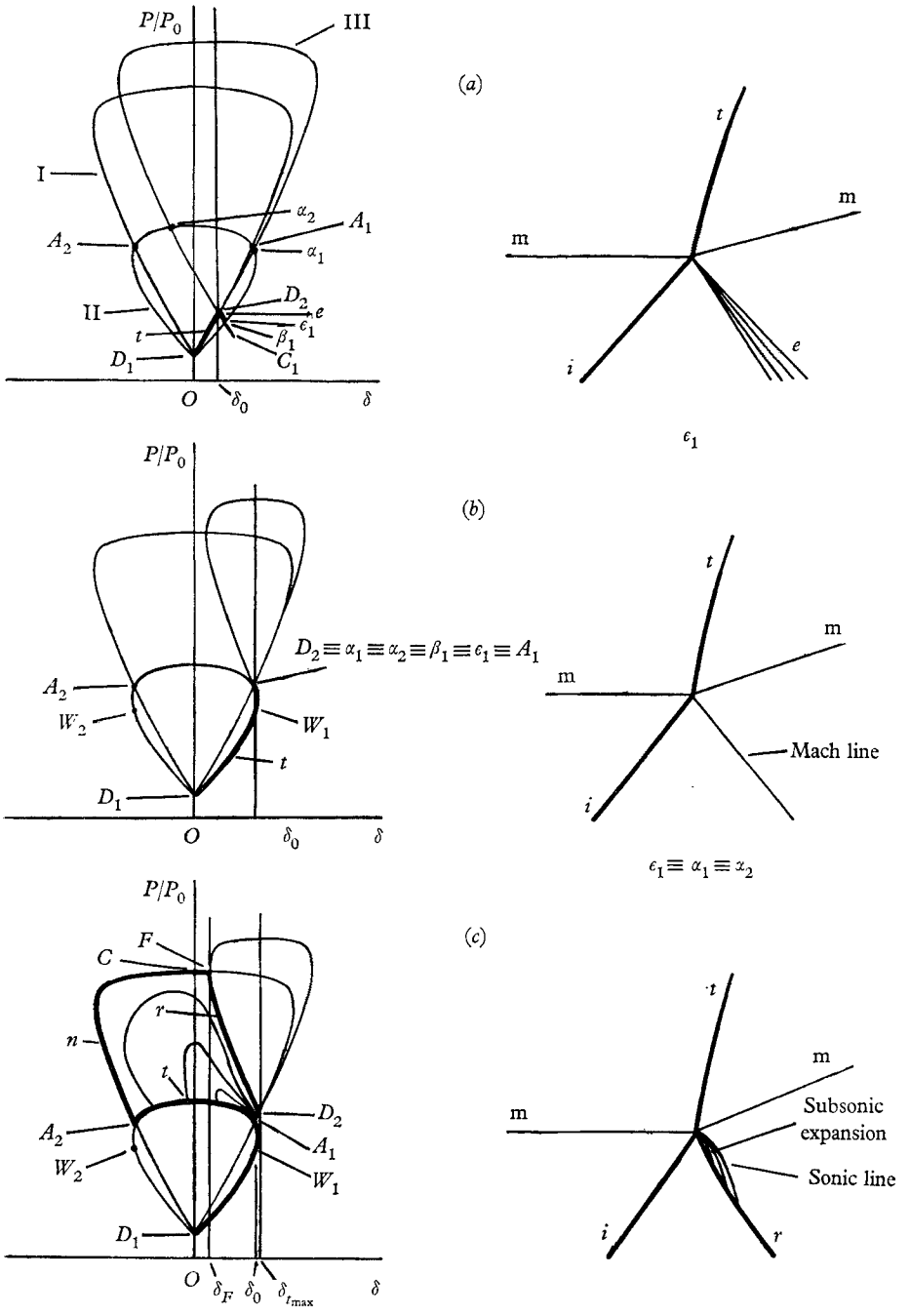

FIGURE 13. For legend see p. 625.

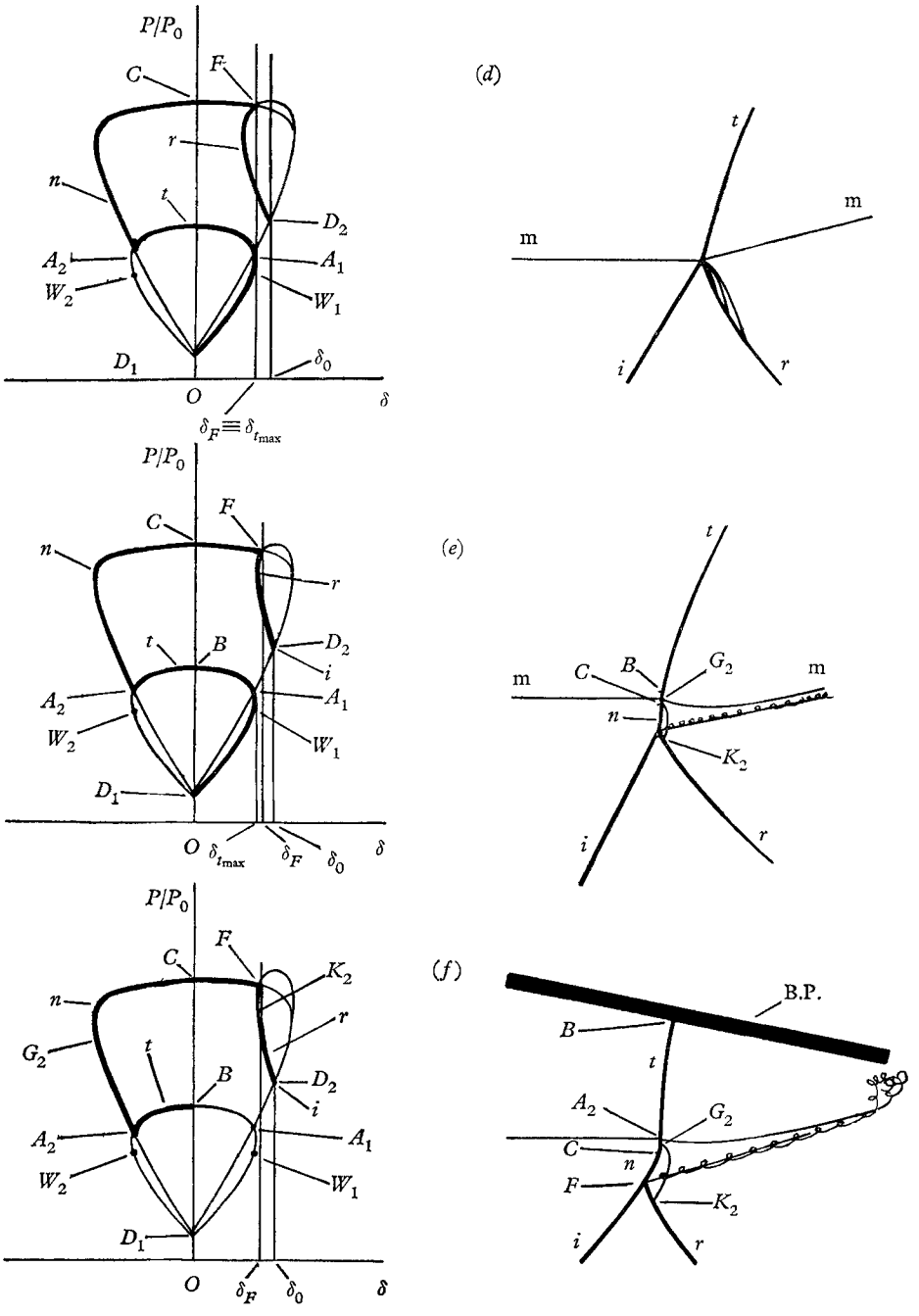

FIGURE 13. For legend see p. 625.

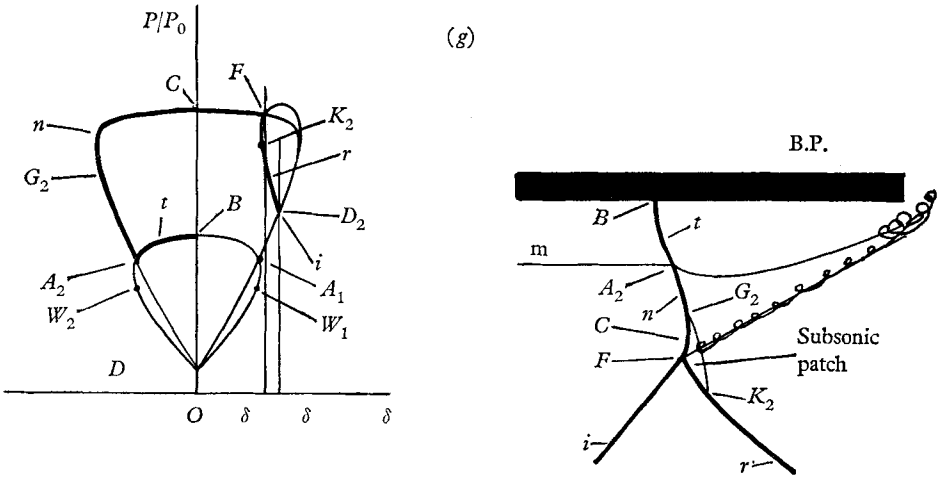

FIGURE 13. Sequence of events resulting from the displacement of polar III from polar I for the refraction of a plane shock i at an air–methane interface in the Mach-number range $M_0 \geqslant 2{\cdot}25$.

line obtained from the computer is shown in figure 10. Further displacement causes β_1 and β_2 to become unreal and the set reduces to (α_1, α_2). The next event of interest is the formation of the coincidence $D_2 \equiv \epsilon_1 \equiv \alpha_1 \equiv \alpha_2 \equiv A_1$ and the corresponding double root $\alpha_1 \equiv \alpha_2$, obtained from the computer, is also shown in figure 10. At this condition the reflected shocks of the α_1 and α_2 solutions are Mach line degeneracies. With any further displacement α_1 and α_2 lose their physical significance and their place is taken by the unique solution ϵ_1. The double-root line $\alpha_1 \equiv \alpha_2$ is thus a boundary between a regular refraction with a reflected shock and a regular refraction with a reflected expansion. The ϵ_1 solution begins with a Mach line degeneracy at the above coincidence and finally ends as a sonic degeneracy at the coincidence $D_2 \equiv \epsilon_1 \equiv V_1$. Beyond this last coincidence an irregular system is to be expected. Hence for the range $1{\cdot}38 \leqslant M_0 \leqslant 2{\cdot}0$ the sonic line is a boundary between a regular refraction with a reflected expansion and an irregular refraction.

For the Mach-number range $2{\cdot}0 \leqslant M_0 \leqslant 2{\cdot}5$ there is only one essential change in the sequence compared with the one shown in figure 15. Over this range the computer results show that there is the coincidence $A_1 \equiv V_1$, which means that the double-root line $\alpha_1 \equiv \alpha_2$ coincides with the sonic line as shown in figure 10. The physical consequence is that the ϵ_1 solution is now degenerate but otherwise the sequence is similar to that of figure 15. The next sequence, figure 16, is typical of the Mach-number range $2{\cdot}5 \leqslant M_0 \leqslant 2{\cdot}92$ and here the computer shows that the sonic point V_1 is below the polar intersection A_1. In consequence, the double-root line $\alpha_1 \equiv \alpha_2$ is slightly below the sonic line in figure 10. Continued displacement now causes the α_1 and α_2 roots to become unreal after the $\alpha_1 \equiv \alpha_2$ coincidence has been formed. The physical result is that, instead of forming Mach line degeneracies, the reflected shocks of the α_1 and α_2 refractions actually have finite strength at the double root. A somewhat similar situation was encountered in figure 11 (*c*). Further differences in the polar diagrams arise when $M_0 \geqslant 2{\cdot}92$ and

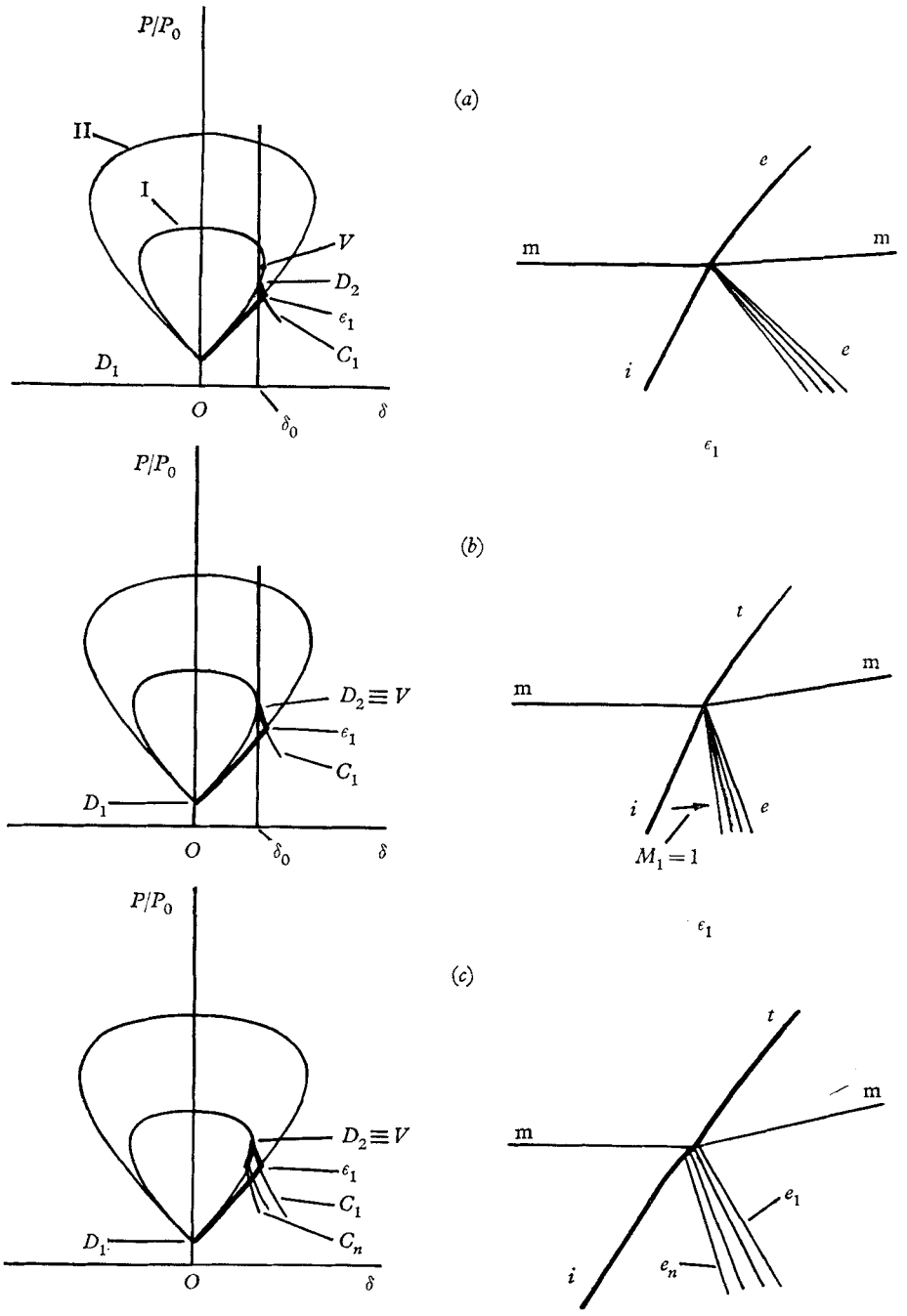

FIGURE 14. Sequence of events resulting from the displacement of the characteristic C_1 from the point D_1 for the refraction of a plane shock at an air–carbon dioxide interface in the Mach-number range $M_0 \leqslant 1{\cdot}38$.

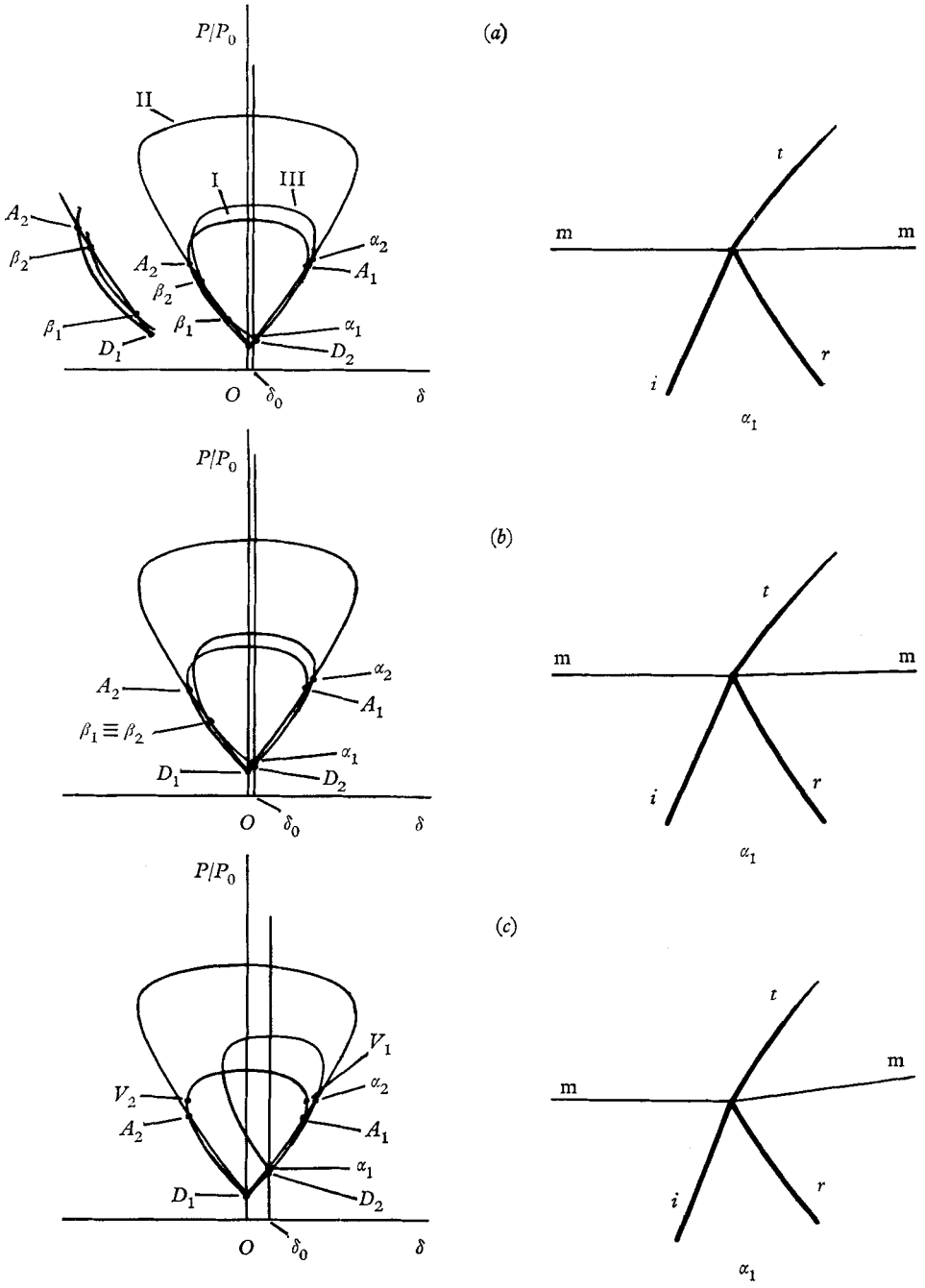

FIGURE 15. For legend see page 628.

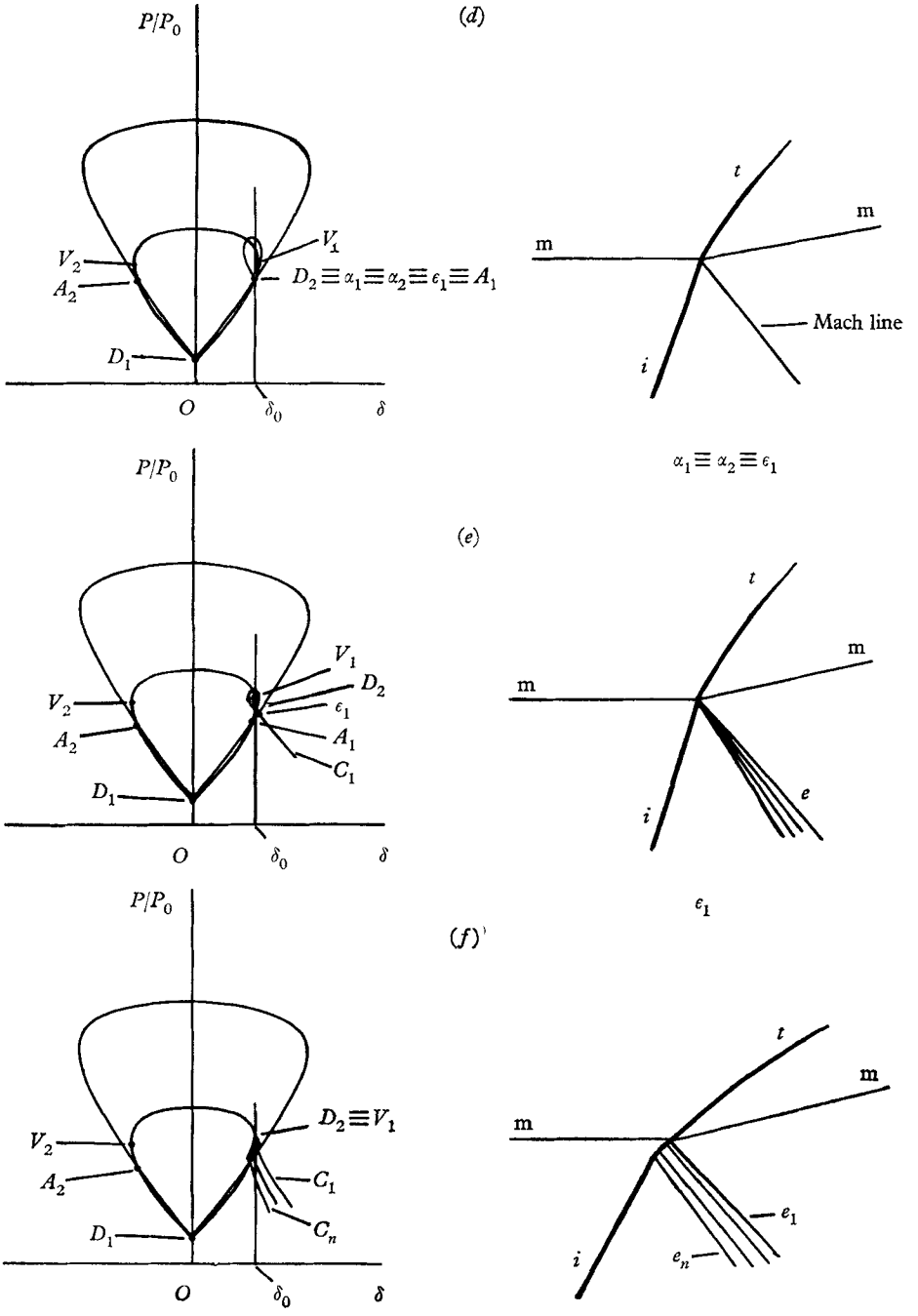

FIGURE 15. Sequence of events resulting from the displacement of polar III from polar I for the refraction of a plane shock i at an air–carbon dioxide interface in the Mach-number range $1{\cdot}38 \leqslant M_0 \leqslant 2{\cdot}0$.

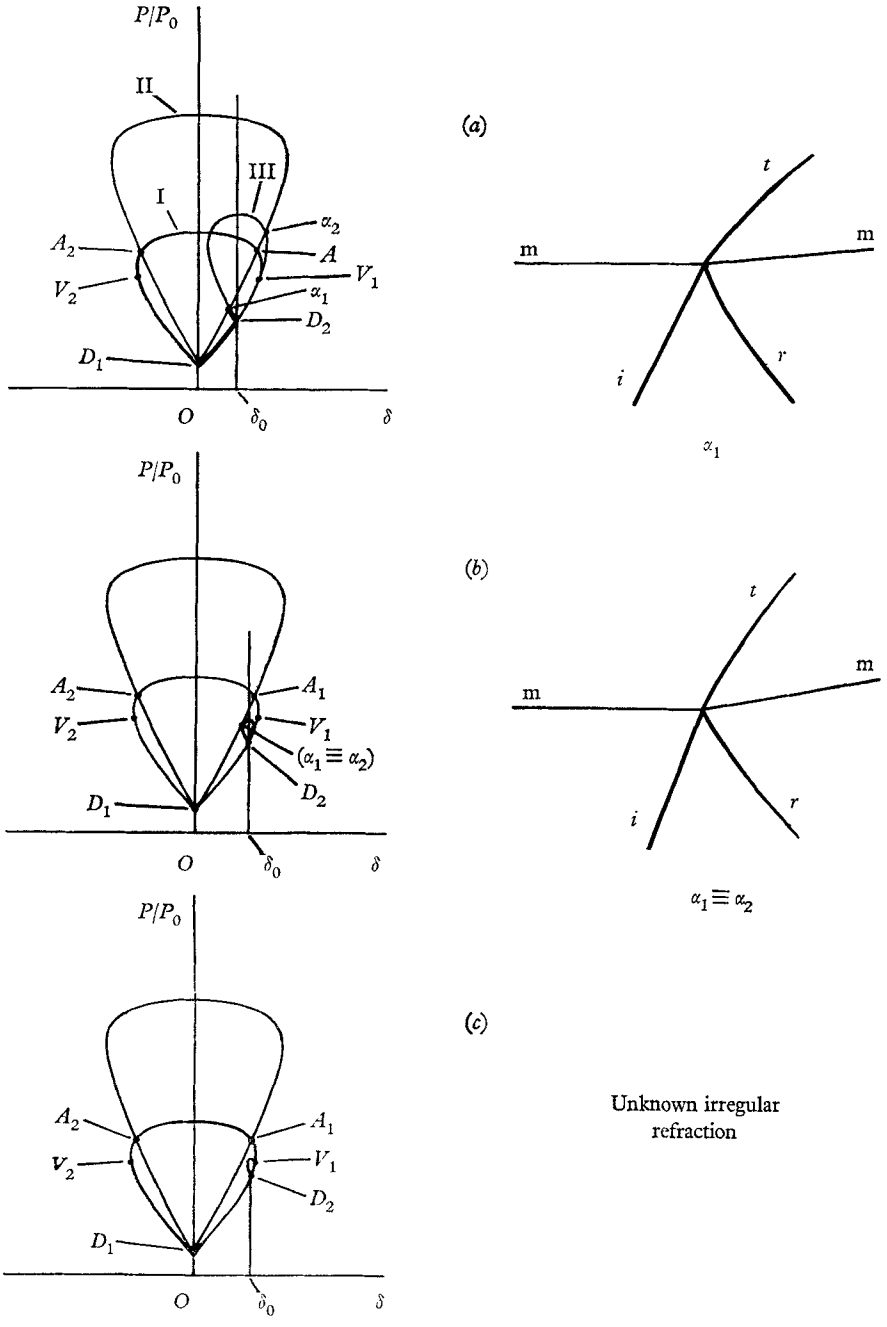

FIGURE 16. Sequence of events resulting from the displacement of polar III from polar I for the refraction of a plane shock i at an air–carbon dioxide interface in the Mach-number range $2{\cdot}5 \leqslant M_0 \leqslant 2{\cdot}92$.

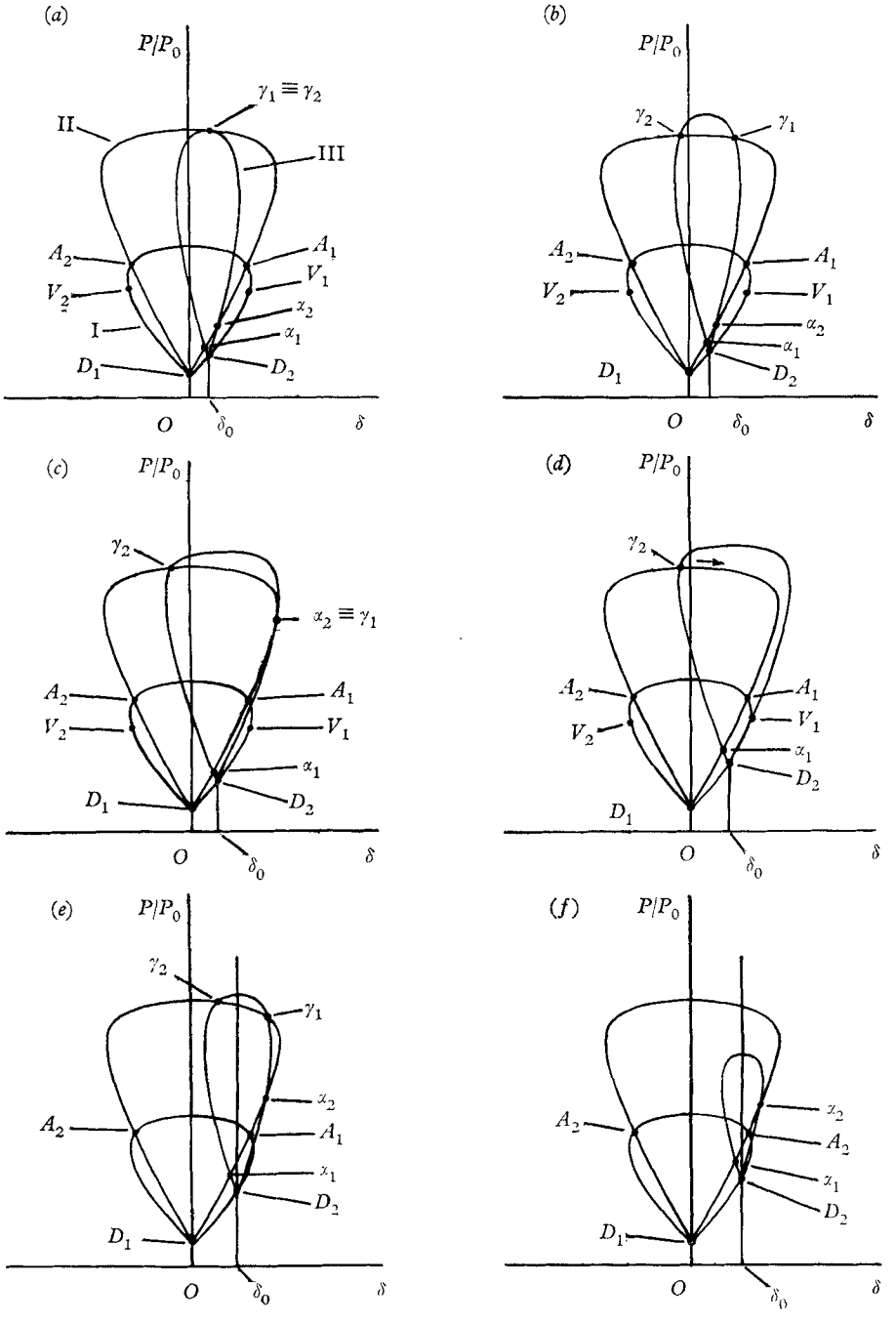

FIGURE 17. For legend see facing page.

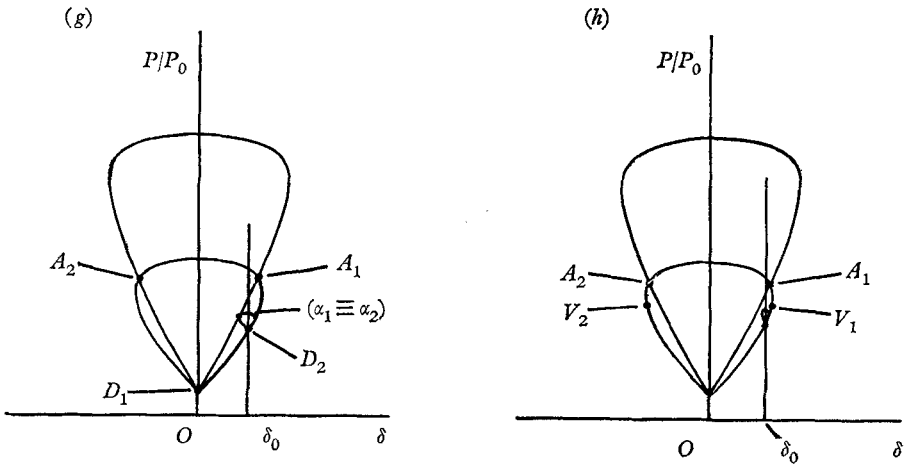

FIGURE 17. Polar diagram sequence resulting from the displacement of polar III from polar I for the refraction of a plane shock i at an air–carbon dioxide interface in the Mach-number range $M_0 \geqslant 2{\cdot}92$.

these are illustrated in figure 17. At first the sequence is similar to those shown in figures 15 and 16, but then with continued displacement the polar for the reflected shock III is found to grow rapidly in the vertical direction until it forms the new intersections γ_1 and γ_2 and the set becomes $(\alpha_1, \alpha_2, \gamma_1, \gamma_2)$. As displacement continues the coincidence $\alpha_2 \equiv \gamma_1$ is formed and these roots then become unreal, reducing the set to (α_1, γ_2). The double roots corresponding to $\gamma_1 \equiv \gamma_2$ and $\alpha_2 \equiv \gamma_1$ have been computed and are plotted in figure 10. With continued displacement the polar III eventually begins to shrink and in the approximate range $2{\cdot}92 \leqslant M_0 \leqslant 4{\cdot}0$ this causes α_2 and γ_1 to become real again. In these circumstances continued displacement next results in the coincidence $\gamma_1 \equiv \gamma_2$ and then these roots become unreal. Finally, one obtains $\alpha_1 \equiv \alpha_2$ and these roots also become unreal. At first sight this sequence may seem complicated but it is easily deduced from the curves of figure 10.

6. The multiplicities and their physical significance

At this stage it would be desirable to devise further tests for the physically significant roots shown in figures 7 and 8 so that they could be eliminated one at a time until only a unique solution remained. If the tests were correctly based, then it would be this solution that would appear in an actual experiment. While at present it does not seem to be possible to attain this ideal state, an additional physical argument can be brought to bear which gives a plausible reason for selecting a particular solution from the ordered set. Consider, for example, the situation shown in figure 11 (*a*), (*b*) where both the α_1 and α_2 solutions exist and the problem is to decide which one of them will appear in an experiment. The argument that will be used here is based on Guderley's (1947) classical discussion of the flow over a wedge. Clearly if the wedge angle is smaller than the attachment angle for the free-stream Mach number then there will be two solutions for the shock wave at the wedge apex. It is well known from experiment that it is

the weaker one that is relevant, but Guderley has given plausible conditions for the appearance of the stronger solution. His discussion cannot be detailed here, but briefly he follows Busemann's idea that there should be an obstruction downstream of the wedge in order to maintain a higher pressure there. Guderley takes this obstruction to be a second wedge whose angle exceeds the attachment angle of the free-stream Mach number. This will be called here a 'strong' disturbance. The second wedge is initially placed well downstream to ensure that the weaker solution appears at the apex of the first wedge. The downstream wedge is then gradually moved upstream until it ultimately forces the weaker solution to change into the stronger solution. It seems reasonable that a similar argument would be valid for the (α_1, α_2) solutions of the shock-refraction problem. In particular, if there are no bodies or boundaries making a strong disturbance in the downstream flow then the weaker α_1 solution is to be selected. This hypothesis will be generalized here by assuming that for any ordered set it will be the weakest solution that will appear when all internal and external boundaries are at infinity.

The usual method mentioned in the literature for resolving the multiplicities is to assume that, in the limit when the incident shock degenerates to a Mach line $P_1/P_0 \to 1$, a physically valid solution must be consistent with the known results of acoustic theory and those that do not satisfy this requirement are discarded. Unfortunately this test, fails for both the air–CH_4 and the air–CO_2 refractions because inspection of figures 7 and 8 shows that at least some of the multiplicities are always preserved at this limit.

7. Comparison of the theory with Jahn's experiments

The computer was used to obtain additional numerical data in a form that was suitable for direct comparison with the experimental results obtained by Jahn. It will be convenient to assume here without loss of generality that Jahn performed a series of experiments in the following sequence. The pressure ratio across the incident shock was held constant and then with the angle of incidence α initially small the experiments were carried out one at a time with successive increases in α until an irregular wave pattern was obtained. Under these conditions increasing the value of α is equivalent to reducing the Mach number M_0.

From figure 9 it is apparent that for the air–CH_4 refraction the effect of reducing M_0 when $\xi = 0{\cdot}85$ or $P_1/P_0 = 1{\cdot}176$ will be a sequence of events similar to that shown in figure 12. The ordered set is initially $(\epsilon_1, \alpha_1, \alpha_2)$, but the α_1 and α_2 solutions will be rejected on the assumption that there are no internal or external boundaries causing a strong disturbance in the flow. The polynomial data are not applicable to the ϵ_1 solution but the adjusted Polachek & Seeger calculations agree well with Jahn's data, figure 3. As α increases the ϵ_1 solution eventually loses its physical significance and the set is reduced to (α_1, α_2). The α_1 solution is selected and the data obtained from the computer agree well with Jahn's data, figure 3. The α_2 results are shown for comparison. When $\xi = 0{\cdot}3$ or $P_1/P_0 = 3{\cdot}33$ the sequence is similar to that shown in figure 13 and initially there is again the set $(\epsilon_1, \alpha_1, \alpha_2)$. The ϵ_1 solution is selected and the adjusted Polachek & Seeger

results again agree well with the experimental data, figure 5. It was pointed out earlier that for this sequence the set is mutually co-extensive so that it is especially interesting to find that there is one experimental point corresponding to an α_2 solution. Two alternative explanations can be offered. First, the boundary conditions may have been altered during the course of the experiments causing a strong disturbance to appear in the flow. This could have been done by altering the position of the back plate. Otherwise the point may represent an incipient irregular refraction which had not developed sufficiently to cause a measurable deviation from the regular refraction. This explanation appears to be more likely because the initial irregular refraction photographed by Jahn, figure 13 (*c*), is very similar in appearance to the regular refraction.

For the air–CO_2 refraction the sequence of events when $\xi = 0{\cdot}85$ or $P_1/P_0 = 1.176$ is similar to that shown in figure 15. Initially there is the set $(\alpha_1, \beta_1, \beta_2, \alpha_2)$ and then (α_1, α_2), but the α_1 solution is selected in both cases and it agrees well with experiment, figure 3. The α_2 solution was so much stronger that it could not be shown on the same diagram. As α increases the reflected shock eventually degenerates to a Mach line and beyond this condition only the ϵ_1 solution is valid. Here also the adjusted Polachek & Seeger results agree well with experiment. When $\xi = 0{\cdot}3$ or $P_1/P_0 = 3{\cdot}33$ the sequence is again similar to that shown in figure 15, but in this case there is a very limited range for the ϵ_1 solution. The α_1 solution agrees reasonably well with experiment, figure 4, although there is some discrepancy in the range $35° \leqslant \alpha \leqslant 55°$. There is also some difference between the adjusted Polachek & Seeger results and the α_1 results.

8. The irregular wave-refraction systems

Jahn has also used the shock tube to make a study of the irregular wave systems. The objective here will be to find out how far a discussion of these phenomena can proceed on the basis of the hodograph diagram. It will be assumed that the problem can be treated as stationary, which of course is not strictly correct, but it will be approximately true if the essential features of the system are confined within a small region. Although not essential it will help the discussion if for the present all boundaries are assumed removed to infinity. Consider again figure 13, which, it will be recalled, is valid for an incident shock of strength $\xi = 0{\cdot}3$. In figure 13 (*a*) and (*b*) the transmitted shock t maps into the segment $D_1 D_2$ on polar I, while the reflected expansion e maps into the segment $D_2 \epsilon_1$ in figure 13 (*a*) and degenerates into the coincidence $D_2 \equiv \epsilon_1$ in figure 13 (*b*). When the polar III is displaced beyond this coincidence as in figure 13 (*c*) a gap opens into the interior of polar I in the sense that was discussed by Guderley (1947) and Kawamura & Saito (1956). The hodograph map of the wave system is now much extended.† For this condition Jahn observed the wave system shown in the physical plane of figure 13 (*c*). According to the polar diagram the reflected shock at the refraction point should be determined by the point F. This conclusion can be tested against experiment because Jahn has published the necessary data. They have been reproduced here in figure 6. The point F was studied on the

† The mapping technique has been discussed previously in greater detail (Henderson 1965).

computer for $\xi = 0{\cdot}3$ and it was found that it appeared on the subsonic parts of both polars I and III and moreover that the reflected shock had zero curvature at the refraction point. The point F is then what Sternberg (1959) defined as a Group B type intersection. This last fact is important because it indicates that reliable measurements of the reflected shock can be made in the vicinity of the refraction point. The theoretical curve for the point F is compared with the experimental data in figure 6. Agreement is satisfactory for $\alpha < 56°$ but a marked discrepancy develops for a larger value of α. At these larger values of α experiment shows that the wave system is modified by the appearance of a Mach stem n, figure 13 (e), and evidently the discrepancy shown in figure 6 is caused by the growth of this extra wave. A plausible explanation for the growth of the Mach stem can be given on the basis of the polar diagrams as follows.

Referring to figure 13 (c) the total streamline deflexion caused by the incident i and reflected r shocks does not exceed the attachment angle $\delta_{t\max}$ for the transmitted shock t, viz. $\delta_F < \delta_{t\max}$. However, as α continues to increase the polar III shrinks relative to the other polars and this causes δ_F to increase relative to $\delta_{t\max}$ so that eventually $\delta_F = \delta_{t\max}$ as shown in figure 13 (d). If α increases any further then $\delta_F > \delta_{t\max}$ and the deflexion across the transmitted shock t can no longer match the combined deflexions across the shocks i and r. It is suggested that it is this condition that forces the growth of the Mach stem n, figure 13 (e). The shock n is curved and so it is able to make the necessary adjustment between t on the one hand and i and r on the other. The critical condition shown in figure 13 (d) was determined and for $\xi = 0{\cdot}3$ it was found to occur at $\alpha \approx 53°$. Now figure 6 shows that theory and experiment do not begin to deviate significantly until $\alpha > 56°$. This discrepancy can be explained if the Mach stem grows very slowly in the initial stages. Experiments with simple Mach reflexion have indeed shown that the growth of the Mach stem is initially slow (Kawamura & Saito 1956 and Smith 1959), in fact to such an extent that its onset is difficult to detect. In this connexion the interferometer is particularly insensitive and Smith has even described it as 'completely useless in determining the transition between regular and Mach reflexion'. Some criticisms have been levelled at Jahn in this respect (Pack 1964). To complete this aspect of the problem it would be necessary to continue the calculations of the point F into the Mach reflexion system shown in figure 13 (e). However, this requires a knowledge of the angular position of the world line that passes through the point F and the necessary data are not given in Jahn's paper.

The polar diagrams in figure 13 extend into the negative δ half plane once the gap into the interior of polar I has opened. A physical consequence is that both the shocks t and n must be partly inclined forward in the flow. In plate 12 of Jahn's paper the back plate has been set parallel and fairly close to the interface and it evidently makes a strong disturbance in the flow. A sketch of the wave system shown in the photograph is reproduced in figure 13 (g) and there can be no doubt from the original that the shock t inclines forward. In the absence of boundary-layer separation this shock will be locally normal to the back plate and its end-point will map into the point B. The other end-point will be on the gas interface at A_2 where it is joined by the Mach stem n. From the polar diagram it is concluded

that there is continuity in both pressure and streamline direction across the interface at A_2. From A_2 to C the Mach stem is inclined forward with respect to the confluence point F and the original photograph clearly shows that n has the required shape. The polar diagram also shows that in the vicinity of F the flow downstream of both the shocks n and r is subsonic, but further away from F the flow downstream of both shocks is supersonic. This implies the existence of a local subsonic patch at F which is terminated by the sonic line G_2K_2 but the detailed shape of this line cannot be deduced from the polar diagram.

In plate 6 of Jahn's paper or figure 13(f) here, the back plate has been set further away from the interface and at the same time the angle α has been reduced. These changes do not alter the character of the polar diagram, but the photograph shows that some of the above effects are less pronounced. In particular the confluence point F moves closer to the refraction point A_2 and it becomes more difficult to detect the parts of the shocks t and n that are inclined forward. The back plate is evidently having less effect on the flow in the vicinity of the refraction point A_2. In plate 5 of Jahn's paper or figure 13(c) here the situation has been taken a step further with α reduced again and with the boundaries no longer apparently having any effect on the system near A_2. The polar diagram has now been significantly altered in that the condition $\delta_F > \delta_{t\max}$ has now changed to $\delta_F < \delta_{t\max}$ and therefore the point F is able to approach the point A very much more closely. The polar diagram still indicates that n exists and still requires t to be inclined forward at A_2 but neither of these features can be distinguished in the photograph. It is suggested here that the wave systems shown in plate 5 or figure 13(c) and (d) are actually of the form shown in figure 13(e), but that the features of the system in the neighbourhood of BA_2CF are too close together to be resolved by the interferometer. This argument can be strengthened by noting that the streamlines entering the subsonic patch crowd together as they pass out through the gap A_1D_2 in the hodograph plane. According to Kawamura & Saito, who in turn follow Busemann, a region of subsonic flow where the streamlines crowd together corresponds to a region of nearly uniform flow in the physical plane, and by contrast where the streamlines are rare in the hodograph plane then there is a region of rapidly changing flow properties in the physical plane. If this idea is applied to the refraction problem shown in figure 13(e) then just after transition it would be concluded that the region BA_2CF would be shrunk almost to a point in the physical plane and the observed flow would be dominated by the conditions at A_1.

If now ξ is increased the effect on the polar diagram is for the intersections A_1 and A_2 to move towards D_1 so that eventually they will coincide with the sonic points W_1 and W_2 of polar II and with any further increase in ξ they will move on to the supersonic part of II. Attempts to construct a polar diagram for this condition were not very satisfactory from the physical point of view. Guderley (1947) during a discussion of transonic wave systems has even expressed the opinion that this type of intersection is physically meaningless and suggests that instead the polars should be joined by a characteristic curve. This idea has been adopted here and the curve c_1 has been constructed in figures 12(e) and (f); it begins at the sonic point W_2. When ξ increases from 0·3 as in figure 13(e) to 0·85 as in figure 12(f)

the following physical changes are indicated. Once the refraction point A_2 enters the supersonic region of II, expansion waves are generated at this point. These waves intersect the Mach stem n and cause the sonic point G_2 to move towards the confluence point F and eventually to join it. With continued development there is ultimately supersonic flow downstream of the entire length of n and this makes it possible for an additional shock j to propagate from F into the flow downstream of n. A fourth polar must then be added to the hodograph diagram to accommodate j as in figure 12(f). Jahn has published two photographs, plates 7 and 8 of his paper, of wave systems similar to that shown in figure 12(f) but the present writer cannot decide from them if the expansion e_1 is present, although the wave n in plate 7 does have the required shape. If the expansion is present then the Mach number downstream of n will be variable and the map of j will deviate somewhat from the polar segment shown. The sonic lines s_1 and s_2 will also be present if the pressure immediately downstream of the waves is sufficiently larger than the ambient pressure far downstream. Both sonic lines are present in plate 7 of Jahn's paper.

Jahn found the irregular wave systems for the air–CO_2 interface to be much less complicated than for the air–CH_4 interface. In fact for the two values of $\xi = 0{\cdot}3$, $0{\cdot}85$, and with variable α he found essentially only one irregular system. For $\xi = 0{\cdot}85$ the theory predicts that the irregular system will begin to appear once the point D_2 has reached and then passed the sonic point V_1 on polar I as in figure 15(e), (f). The system photographed by Jahn has been sketched in the physical plane of figure 15(f). The shock i is curved near the interface and in this region it emits a continuous band of expansion waves. This means that α decreases along the shock and presumably becomes a minimum at the interface. The solution at the interface has been constructed in the hodograph plane and it will determine both the shock t and the expansion e_1. However, because the Mach number M_0 varies along i, the maps of i and of the expansion band e_1–e_n are not simple. The sequence shown in figure 15 is also relevant to the shock of strength $\xi = 0{\cdot}3$. There appears to be no physically significant difference indicated either theoretically or experimentally between the irregular systems for $\xi = 0{\cdot}3$ and $0{\cdot}85$. These were the only wave strengths mentioned in Jahn's paper but from figure 10 it will be noticed that for $M_0 > 2{\cdot}5$ or $\xi < 0{\cdot}16$ the polar diagram must have different character when the system becomes irregular. The diagrams are shown in figures 16 and 17. Consequently it is possible that a new type of irregular system may appear for these stronger incident shocks.

9. Concluding remarks

The use of the polar diagram has the advantage of bringing some order and coherence to the quite complicated phenomena that were observed in Jahn's experiments. However, there is need of some additional experiments and these should preferably be carried out with the help of a shadowgraph or Schlieren system as well as an interferometer. Among the problems that need to be explored in more detail is the growth of the Mach stem. This requires in particular more data of the type shown in figure 6 with, in addition, some information on the

angular position of the shock confluence point F. Another problem is that of the transition from the Mach-reflexion type of irregular refraction for $\xi = 0{\cdot}3$ to the more complex type for $\xi = 0{\cdot}85$ and it would be of especial interest to find out if the transition is brought about by the appearance of an expansion fan at the refraction point A_2. To augment and perhaps complete the picture of the irregular refraction types it also seems to be necessary to photograph the irregular system for the air–CO_2 interface when $\xi < 0{\cdot}16$. This experiment may reveal a previously unknown phenomenon.

REFERENCES

GUDERLEY, K. G. 1947 Considerations of the structure of mixed subsonic–supersonic flow patterns. *Tech. Rept* F-TR-2168-ND, Headquarters Air Materiel Command, Wright Field, Dayton, Ohio.

GUDERLEY, K. G. 1962 *The Theory of Transonic Flow*. Oxford: Pergamon Press.

HENDERSON, L. F. 1964 *Aero Quart.* **15**, 181.

HENDERSON, L. F. 1965 *Aero. Quart.* **16**, 122.

HENDERSON, L. F. 1966 *Aero. Quart.* **17**, 1.

HILSENRATH J., BECKETT, C. W., BENEDICT, W. S., FANO, L., HODGE, H. J., MASI, J. F., NUTTALL, R. L., TOULOUKIAN, Y. S. & WOOLLEY, H. W. 1960 *Tables of Thermodynamic and Transport Properties*. Oxford: Pergamon Press.

JAHN, R. G. 1956 *J. Fluid Mech.* **1**, 457.

KAWAMURA, R. & SAITO, H. 1956 *J. Phys. Soc. Japan* **11**, 584.

MCBRIDE, B. J., HEIMEL, S., EHLERS, J. G. & GORDON, S. 1963 *NASA* no. SP-3001.

PACK, D. C. 1964 *J. Fluid Mech.* **18**, 549.

POLACHEK, H. & SEEGER, R. J. 1951 *Phys. Rev.* **84**, 922.

SMITH, W. R. 1959 *Phys. Fluids* **2**, 533.

STERNBERG, J. 1959 *Phys. Fluids* **2**, 179.